# Motion and Deformation Estimation from Medical Imagery by Modeling Sub-Structure Interaction and Constraints

Ganesh Sundaramoorthi
*Dept. of Electrical Engineering & Dept. of Applied Mathematics and Computational Science*
*King Abdullah University of Science and Technology (KAUST), Saudi Arabia* (ganesh.sundaramoorthi@kaust.edu.sa)

Byung-Woo Hong
*Computer Science Department, Chung-Ang University, Seoul, Korea* (hong@cau.ac.kr)

Anthony Yezzi
*School of Electrical and Computer Engineering, Georgia Institute of Technology, Atlanta, USA* (ayezzi@ece.gatech.edu)

ABSTRACT: This paper presents a novel medical image registration algorithm that explicitly models the physical constraints imposed by objects or sub-structures of objects that have differing material composition and border each other, which is the case in most medical registration applications. Typical medical image registration algorithms ignore these constraints and therefore are not physically viable, and to incorporate these constraints would require prior segmentation of the image into regions of differing material composition, which is a difficult problem in itself. We present a mathematical model and algorithm for incorporating these physical constraints into registration / motion and deformation estimation that does not require a segmentation of different material regions. Our algorithm is a joint estimation of different material regions and the motion/deformation within these regions. Therefore, the segmentation of different material regions is automatically provided in addition to the image registration satisfying the physical constraints. The algorithm identifies differing material regions (sub-structures or objects) as regions where the deformation has different characteristics. We demonstrate the effectiveness of our method on the analysis of cardiac MRI which includes the detection of the left ventricle boundary and its deformation. The experimental results indicate the potential of the algorithm as an assistant tool for the quantitative analysis of cardiac functions in the diagnosis of heart disease.

## 1 INTRODUCTION

Registration of medical images is of utmost importance for a number of applications in medicine. Typically, medical images are composed of many interacting parts and sub-structures, and each of these parts have different physical laws governing their motion and deformation (or at least different parameters from the same governing equations). For example, in the case of cardiac MRI registration, the deformation of ventricles and the myocardium (heart muscle) satisfy different governing equations because of differing material composition. Therefore, in order to correctly register medical images, one must first segment or detect each of the sub-structures where different governing laws hold, and then register the sub-structures based on the equation that holds for the particular sub-structure. Of course, now the problem becomes performing the segmentation. Current methods for medical image registration assume that the segmentation is given (usually done by hand or segmentation techniques in hardware, see for example, [5, 2, 12]) or completely ignore this problem, register the images directly, and hope that good choices of regularization can overcome this predicament ([17, 16, 9]). Even when manual segmentation is done perfectly, and when the registration is performed correctly (which is highly unlikely due to noise and modeling errors) in each sub-structure, there is no guarantee that physical constraints for the deformation across sub-structures are satisfied.

In this work, we propose a novel registration method that models materials of different composition and therefore differing laws of deformation in each of the sub-structures composing the image, and the physical constraints of the deformation that must occur across sub-structures. We accomplish this by automatically detecting (segmenting) sub-structures using their *discriminating dynamics or deformation*. The deformation in each sub-structure is simultaneously computed while the sub-structures are estimated. Further, physical constraints across sub-structures are naturally incorporated into a unified optimization framework for the deformation and the sub-structure segmentation. Although our framework is valid in a number of registration scenarios (e.g., brain registration), we demonstrate the idea on the analysis of cardiac MRI, of critical importance [14, 2, 12], which includes the detection of the left ventricle boundary, its deformation, and the deformation in the surrounding area, i.e., the myocardium. For simplicity, we illustrate the formulation on an image comprosed of two sub-structures, although the formulation may be similarly extended to any number of sub-structures.

## 2 MATHEMATICAL METHODOLOGY

In this section, we formulate a mathematical model for registering medical images (and determining motion and deformation of objects within the image) under the assumption that several objects and/or sub-parts that are composed of different materials are imaged. This is the case, for example, in brain MRI (white / gray matter) and cardiac MRI (ventricles / myocardium). We model differing dynamics among sub-parts and the constraints that are imposed across the common boundaries of sub-parts.

### 2.1 Interaction Between Inhomogeneous Materials

We start by considering the most basic assumption governing deforming objects typical in medical imagery, that is, the conservation of mass. This assumption is reasonable for cardiac MRI, and is a good approximation in other cases of interest. The assumption is not central to the thesis of the work, which is to model the constraints and interactions among neighboring sub-parts, and our method is general and can be used with other governing equations. We will see however, that the mass conservation property leads to the standard equations that are typically used in image registration.

We assume that the domain of the object(s) of interest is $\Omega \subset \mathbb{R}^n$ (where $n = 2$ or $n = 3$ depending on whether we wish to model in two or three dimensions). Within a homogeneous material (e.g., the myocardium or ventricle in cardiac MRI) of an object, the differential form of the conservation of mass implies the continuity equation:

$$\rho_t + \text{div}\,(\rho v) = 0 \tag{1}$$

where $\rho : [0,1] \times \Omega \to \mathbb{R}^+$ denotes the density of the material and $v : [0,1] \times \Omega \to \mathbb{R}^n$ denotes the infinitesimal velocity of the material, $\rho_t$ denotes differentiation with respect to the first variable, and div () indicates the divergence operator. The first parameter of $\rho$ and $v$ is time denoted by $t$, and the second parameter $x$ indicates spatial location. Note that the above equation holds within regions of the same material characteristics, but *not across* material boundaries. Noting that tissue is composed mostly of water and therefore, can be considered as an incompressible fluid [15], we have that

$$\text{div}\,(v) = 0, \tag{2}$$

and therefore, (1) reduces to

$$\rho_t + \nabla\rho \cdot v = 0 \tag{3}$$

within materials of the same material composition. Here $\nabla\rho$ denotes the spatial gradient (derivative with respect to $x$). We may replace $\rho$ in (3) with the image intensity $I : [0,1] \times \Omega \to \mathbb{R}^+$ since in many imaging modalities such as MRI and CT, the intensity represents a conserved quantity [15] via roughly proportionality to the density, and thus

$$I_t + \nabla I \cdot v = 0. \tag{4}$$

The above equation is equivalent to the differential form of the *brightness constancy equation* [11] for two-dimensional images which is commonly used in the computer vision literature.

Assuming that the input image is composed of two differing material regions (for example, the myocardium and ventricles in cardiac MRI), we have that

$$\begin{cases} I_t(t,x) + \nabla I(t,x) \cdot v_{in}(t,x) = 0 & x \in \text{int}\,(R_t) \\ I_t(t,x) + \nabla I(t,x) \cdot v_{out}(t,x) = 0 & x \in \text{int}\,(\Omega \backslash R_t) \end{cases} \tag{5}$$

where $\Omega$ is the domain of the image, $R_t \subset \Omega$ denotes the first material region (as a function of $t$), and $v_{in}$ and $v_{out}$ (defined on $R_t$ and $\Omega \backslash R_t$, respectively) denote the velocities inside $R_t$, the first region, and $\Omega \backslash R_t$, the second material region. The notation int $(R_t)$ indicates the interior of the set $R_t$ (not including the boundary). The formulation may be similarly extended to any number of material regions, but we choose to illustrate our technique on two regions for simplicity.

Note that the differing statistics of $v_{in}$ and $v_{out}$ due to material differences make determining the unknown $R_t$ possible. The solution of (5) is not unique and therefore, regularization is required, as typical in determining optical flow in computer vision. Even with typical regularization (for example, assumption of spatial smoothness of the velocity fields), the equations (5) still do not yield a unique solution without specification of a boundary condition on $\partial R_t$, the boundary of $R_t$, which is an extra condition not needed in optical flow problems. However, this can be resolved by noting the physical constraint that the velocity (not the density $\rho$) must be continuous across the boundary $\partial R_t$ of material regions:

$$v_{in}(t,x) = v_{out}(t,x),\ x \in \partial R_t. \tag{6}$$

The constraint above makes it possible to solve (5) directly on $\partial R_t$ when the image is two-dimensional. Indeed, one can show, by solving (5) and (6) directly on $\partial R_t$, that

$$v_b(t,x) = I_t(t,x) \frac{(\nabla I_{in}(t,x) - \nabla I_{out}(t,x))^\perp}{\nabla I_{in}(t,x) \cdot \nabla I_{out}(t,x)^\perp},\ x \in \partial R_t \tag{7}$$

where $v_b(t,x) = v_{in}(t,x) = v_{out}(t,x)$, $x \in \partial R_t$, $w^\perp$ denotes a vector perpendicular to $w$, and $\nabla I_{in}$ and $\nabla I_{out}$ denote the limits of the gradients approaching the boundary $\partial R_t$ from within int $(R_t)$ and int $(\Omega \backslash R_t)$, respectively. The expression holds when $\nabla I_{in}$ and $\nabla I_{out}$ are non-parallel, and are non-zero. In other words, the expression breaks down when there is no discontinuity of the gradient angle of the image across the material boundary. The expression also holds in three-dimensions except the expression no longer yields a unique solution.

### 2.2 Energy-Based Formulation for Registration

In order to determine the registration between images in the sequence, one would need to determine the velocity field $v$ for each time $t$ at every spatial location. The registration (cumulative motion/deformation between two images) $\phi : [0,1] \times \Omega \to \Omega$ between the image at time zero and time $t$ can be obtained by integration:

$$\phi(t,x) = x + \int_0^t v(\tau, \phi_\tau(x))\,\mathrm{d}\tau, \tag{8}$$

where $v|R_t = v_{in}$, $v|\Omega \backslash R_t = v_{out}$, and $v|\partial R_t = v_b$. Therefore, we need to determine $v_{in}, v_{out}$. Note that since $v_{in}$ is supported on $R_t$ and $v_{out}$ is supported on $\Omega \backslash R_t$, $R_t$ either must be known or it must be estimated from the data. Our approach is to jointly estimate $v_{in}, v_{out}$ and $R_t$ as part of an optimization problem.

We setup an optimization problem incorporating the conditions (5) and the constraint (6). The energy that we

propose is

$$E(R, v_{in}, v_{out}, v_b) = \int_0^1 \int_{R_t} f_{in}(v_{in}(t,x))\,\mathrm{d}x\,\mathrm{d}t + \int_0^1 \int_{\Omega\setminus R_t} f_{out}(v_{out}(t,x))\,\mathrm{d}x\,\mathrm{d}t + \int_0^1 \int_{\partial R_t} f_{bndry}(v_b(t,x))\,\mathrm{d}S(x)\,\mathrm{d}t \tag{9}$$

where $v_b$ is the velocity defined on $\partial R_t$ for all $t$, and $\mathrm{d}S$ denotes the surface area element (or arclength element if $n = 2$). Further, the optimization is subject to the constraint $v_b(t,x) = v_{in}(t,x) = v_{out}(t,x)$, $x \in \partial R_t$. An auxiliary variable $v_b$ has been added to the energy in order to simplify imposing the constraint (6). The functions $f$ are defined as follows :

$$f_{in}(v_{in}) = (I_t + v_{in} \cdot \nabla I)^2 + \text{Reg}(v_{in}) \tag{10}$$

$$f_{out}(v_{in}) = (I_t + v_{out} \cdot \nabla I)^2 + \text{Reg}(v_{out}) \tag{11}$$

$$f_{bndry}(v_b) = (I_t + v_b \cdot \nabla I_{in})^2 + (I_t + v_b \cdot \nabla I_{out})^2 + \text{Reg}(v_b) \tag{12}$$

where Reg indicates a regularization term that includes spatial and time regularity, e.g., $\text{Reg}(v_{in}) = |\nabla v_{in}|^2 + |\partial_t v_{in}|^2$. Further, another constraint that is imposed is

$$R_t = \phi(t, R), \tag{13}$$

that is, the region at time $t$ is obtained by warping the initial region $R$ along the velocity field. Note that we exclude weighting in (9) each of the terms for ease of presentation, but they are used in practice.

The use of regularization of $v_{in}$ and $v_{out}$ as seen above is to regularize the brightness constancy equation (such a motion prior is realistic since the motion within homogeneous regions in medical imagery is smooth spatially and in time). The sophisticated deformation in many organs (e.g., the heart) makes the use of TV regularization [4], which favors piecewise constant motion and therefore popular in computer vision, unsuitable. We choose not to incorporate the closed form solution (7) directly, but instead incorporate the constraint (6) and (5) into the term $f_{bndry}$. Therefore, the portion of the energy due to the term $f_{bndry}$ is small when the constraints are satisfied. Due to noise, pointwise estimates of $v_b$ using (7) may not provide an accurate estimate of $v_b$ and when $\nabla I_{in}$ and $\nabla I_{out}$ are close to parallel, numerical problems may arise, and therefore, we work with the constraints directly and further add regularity of the velocity along the boundary as in $f_{bndry}$.

In order to simplify matters for optimization, we assume $n = 2$ (the image is two-dimensional), omit regularization of the vector fields $v_{in}, v_{out}, v_b$ and $R_t$ in time and the constraint $R_t = \phi(R)$, and in this case, the region and velocities can be computed by optimizing the following energy for each time $t$:

$$E(R, v_{in}, v_{out}, v_b) = \int_R \left[(I_t + v_{in} \cdot \nabla I)^2 + |\nabla v_{in}|^2\right] \mathrm{d}x + \int_{\Omega\setminus R} \left[(I_t + v_{out} \cdot \nabla I)^2 + |\nabla v_{out}|^2\right] \mathrm{d}x + \int_{\partial R} \mathrm{d}s + \int_{\partial R} \left[(I_t + v_b \cdot \nabla I_{in})^2 + (I_t + v_b \cdot \nabla I_{out})^2 + |(v_b)_s|^2\right] \mathrm{d}s$$

$$\text{subject to } v_b = v_{in} = v_{out} \text{ on } \partial R. \tag{14}$$

The variable $s$ denotes the arclength parameter of $\partial R$, and $(v_b)_s$ denotes the derivative with respect to the arclength. We suppress the time variable in $R_t$ and the velocities in the above energy for convenience. The integral over time has been eliminated since $R_{t'}$ and the velocities at time $t'$ are treated as independent of $R_t$ and the velocities at time $t$. The formulation assumes that the images are sampled fine enough in time so that the motion/deformation between frames is small. This is realistic in cardiac MRI, which we test in the experiments. Larger deformations between consecutive frames can be handled using multiscale methods and/or ideas in [5], but we forgo this to illustrate the main concept of modeling interactions between different materials and constraints across material boundaries.

### 2.3 Relation of the Model to Existing Work

The first two terms of the energy (14) are reminiscent of the energy used in Motion Competition [8] in computer vision where the objective is to segment objects that move with differing velocities. Each of the objects are described by parametric motions. We do not restrict the model of motion to simple parametric models such as translations or affine motions, as the motion of the heart is much more sophisticated, and further the velocity in our model is continuous across $\partial R$ (although the derivatives need not be), something that has not been considered before and requires added reasoning and sophistication. Each of the first two terms of the energy (14) are identical to Horn & Schunck optical flow [11], however, we extend the model to model discontinuities in the gradient of the velocity field across (unknown) material boundaries. One can think of our model as an extension of the Mumford and Shah model [13] to deformations with an added physical constraint of continuous (and not differentiable) motion across boundaries.

The energy (9) can be thought of as a generalization of the popular Large Deformation Diffeomorphic Metric Mapping (LDDMM) [5] framework used in medical image registration. In LDDMM, only one region $R = \Omega$ is assumed, and therefore, constraints across boundaries of differing materials are not considered. The first term of (9) with the constraint (8) is similar to the energy considered in LDDMM, and regularization across material boundaries is performed - an undesirable property. Our framework can include multiple differing material regions, and these re-

gions are estimated as part of the optimization process. Our energy (9) is also related to the Riemannian formulation of optimal mass transport methods for image registration [10]. In those methods, $R = \Omega$ and the first term of (9) that contains the term $I_t + \nabla I \cdot v_{in}$ is the mass preservation constraint used in [10] with the additional constraint of incompressible motion. The regularization of $v_{in}$ differs in mass transport methods, however, and the penalty is on the magnitude of $v_{in}$ rather than $\nabla v_{in}$, as in our case.

### 2.4 Optimization Method

We now present a method to optimize the energy in (14). The optimization of $E$ consists of an alternating minimization in $v_b$, $v_{in}, v_{out}$, and $R$. First, fixing $R$, $v_{in}, v_{out}$ and optimizing in $v_b$ through variational calculus, we find the following condition, which is an ODE defined on $\partial R$, and ensures a global optimum for a given $R$:

$$-(v_b)_{ss} + (\nabla I_{in} \nabla I_{in}^T + \nabla I_{out} \nabla I_{out}^T) v_b = \\ -I_t(\nabla I_{in} + \nabla I_{out}) \quad (15)$$

with circular boundary conditions. The subscripts in the expression $(v_b)_{ss}$ denotes the second derivative with respect to the arclength parameter of $\partial R$. The above equation can be discretized as a sparse linear system and can be solved efficiently.

The vector field $v_b$ that is defined on $\partial R$ is the boundary condition for $v_{in}$ and $v_{out}$, and with this condition, we may optimize $E$ for $v_{in}$ and $v_{out}$ holding $v_b$ and $R$ fixed. The global optimum solution for the given $R$ and $v_b$ is given by the solution of the following decoupled PDE:

$$\begin{cases} -\Delta v_{in} + \nabla I \nabla I^T v_{in} = -I_t \nabla I & \text{on int}\,(R) \\ -\Delta v_{out} + \nabla I \nabla I^T v_{out} = -I_t \nabla I & \text{on int}\,(\Omega \backslash R) \\ v_{in} = v_{out} = v_b & \text{on } \partial R, \end{cases} \quad (16)$$

We impose the standard Neumann boundary conditions for $v_{out}$ on $\partial\Omega$, as typical in optical flow problems. These PDE can be solved efficiently using a conjugate gradient solver as (16) forms a positive definite linear system.

Finally, holding $v_b, v_{in}, v_{out}$ fixed, one can solve for $R$ using an iterative technique, and for simplicity, we use a gradient descent to optimize $E$ in $R$ (see [6, 7]), although other methods may be used (e.g., [3]). Setting $c = \partial R$, the gradient descent equation is

$$\partial_\tau c = \left[ (I_t + v_b \cdot \nabla I_{in})^2 - (I_t + v_b \cdot \nabla I_{out})^2 \right. \\ \left. + |\nabla v_{in}|^2 - |\nabla v_{out}|^2 + \kappa \right] \mathcal{N} \quad (17)$$

where $\mathcal{N}$ denotes the inward normal vector of $c$, $\kappa$ denotes the curvature of $c = \partial R$, and $\tau$ denotes an artificial variable that parameterizes the evolution of $c$. Note that the variation of the last term in $E$ (14) is neglected by weighting that term arbitrarily small in this last step of optimizing with respect to $R$.

The optimization algorithm, in summary, is given by the following steps:

1. Initialize $R$
2. Solve the ODE (15) on $\partial R$ for $v_b$
3. Solve the PDE (16) with boundary condition $v_b$
4. Update the region $R$ by an iteration of (17)
5. Repeat Steps 2-4 until convergence of $R$

## 3 EXPERIMENTAL RESULTS

In this section, we present experimental results on real cardiac MRI data to illustrate the performance of our method in determining motion and deformation of the left ventricle (LV) and surrounding areas, and also the left ventricle boundary. Region $R$ will represent the LV and $\Omega \backslash R$ represents everything other than the LV. Therefore, we model only the material differences across the LV boundary. In these experiments, images $I_1$ and $I_2$ at two consecutive time instances are taken from a sequence of cardiac MRI images, and $I_t = I_2 - I_1$, $\nabla I = \nabla I_1$ in the energy $E$. The results obtained by our method are shown in Figure 1. We initialize the region $R$ as a small seed point within the LV, and this is hand initialized. Snapshots of the evolution of $c = \partial R$ representing the LV boundary and the deformation field in the interior, $v_{in}$, and the exterior, $v_{out}$, of the left ventricle are shown in Figure 1 for two different example pairs of images.

We provide comparison to a standard segmentation method [7], the Chan-Vese method, which assumes a piecewise constant distribution of the image intensity and two regions. The segmentation is performed on the image $I_1$. Also, for comparison, we provide standard optical flow results using the Horn-Schunck method [11] to estimate the deformation between the images $I_1$ and $I_2$ (not using the region $R$ at all in the computation). In Figure 1, the top row displays images $I_1$ and $I_2$, the segmentation result obtained by the Chan-Vese method, ground truth for the left ventricle boundary, and the optical flow obtained by the Horn-Schunck model in the standard color coding scheme [1]. The curve evolution for the left ventricle boundary from the initial (left) to the final (right) is presented on the middle row. The registration result obtained by the deformation field at different various time steps, $\tau$, is shown on the bottom row.

The experimental results demonstrate that our model provides an accurate boundary for the left ventricle and the obtained deformation field agrees with the physical motion characteristics of the left ventricle and its surrounding region. The fact that the LV is detected quite accurately indicates also that the deformation is accurate (since inaccurate deformation would lead to errors in estimation of the LV). As can be seen from the deformation recovered by our method, the discontinuity of the gradient of the deformation across the detected LV is clearly sharp and visible, unlike the standard Horn- Schunck method. Our method is shown to be robust to the inhomogeneity of the intensity distribution within the left ventricle. Indeed, the dark regions within the LV are valves, and our method captures them more accurately than segmentation based on intensity

such as the Chan-Vese method. This desirable property is inherited from our model that considers the physical laws of motion and deformation and the interactions and constraints across materials of different chemical composition.

## 4 CONCLUSION

We have proposed a novel general framework for medical image registration in which several objects or sub-parts described by differing material properties are explicitly modeled and the constraints of their motion/deformation across parts are incorporated. This is ignored in prior work on medical image registration to the best of our knowledge, where a common deformation field obeying smoothness properties is assumed on the entire domain of the image, and thus ignoring physical constraints of the deformation field across substructures. As a by-product, our algorithm also automatically determines the sub-structures in a unified optimization framework in which the deformation and boundary of the sub-structures are simultaneously estimated. This not only achieves a more physically plausible registration (estimation of deformation), but also yields the detection of sub-structures, which are of clinical interest in many applications. In our method, the characteristic feature employed in determining the object/ sub-part boundaries is the inhomogeneity of deformation across material boundaries, and thus our method is applicable to objects with sophisticated appearance in which distributions of intensity are not discriminative to distinguish object(s)/sub-parts(s). Objects with such sophisticated appearance are typical in medical images.

To illustrate proof-of-concept, we have implemented a simplified version of our general model (9) which is given by the energy described in (14). In this simplification, we have made the assumption that the deformation across the sequence is uncorrelated, and the region describing an object/sub-part is uncorrelated in time. The simplification leads to a rather simple alternating optimization scheme. The algorithm has been demonstrated on cardiac MRI in the application of detecting the left ventricle and estimating its deformation, although the technique is general for many medical registration scenarios. We have shown that our algorithm accurately detected the left ventricle, provided the deformation that agreed with physical constraints, and estimated the deformation outside the left ventricle in the myocardium region. In comparison to standard intensity-based image segmentation, our method achieves better results, and a more physically plausible deformation. The results demonstrate its effectiveness and potential for quantitative analysis of cardiac functions. Future work includes implementing the full model (9), and testing it on 3D data.

## ACKNOWLEDGEMENT

This work was supported by the Korea Research Foundation Grant (NRF-2010-220-D00078).

## REFERENCES

[1] S. Baker, D. Scharstein, J. Lewis, S. Roth, M. Black, and R. Szeliski. A database and evaluation methodology for optical flow. *International Journal of Computer Vision*, 92(1):1–31, 2011.

[2] A. Bistoquet, J. Oshinski, and O. Skrinjar. Left ventricular deformation recovery from cine mri using an incompressible model. *Medical Imaging, IEEE Transactions on*, 26(9):1136–1153, 2007.

[3] X. Bresson, S. Esedoglu, P. Vandergheynst, J. Thiran, and S. Osher. Fast global minimization of the active contour/snake model. *Journal of Mathematical Imaging and Vision*, 28(2):151–167, 2007.

[4] T. Brox, C. Bregler, and J. Malik. Large displacement optical flow. In *Computer Vision and Pattern Recognition, IEEE Conference on*, 2009.

[5] Y. Cao, M. Miller, R. Winslow, and L. Younes. Large deformation diffeomorphic metric mapping of vector fields. *Medical Imaging, IEEE Transactions on*, 24(9):1216–1230, 2005.

[6] V. Caselles, R. Kimmel, and G. Sapiro. Geodesic active contours. *International journal of computer vision*, 22(1):61–79, 1997.

[7] T. Chan and L. Vese. Active contours without edges. *Image Processing, IEEE Transactions on*, 10(2):266–277, 2001.

[8] D. Cremers and S. Soatto. Motion competition: A variational approach to piecewise parametric motion segmentation. *International Journal of Computer Vision*, 62(3):249–265, 2005.

[9] P. Ghosh, M. Sargin, and B. Manjunath. Generalized simultaneous registration and segmentation. In *IEEE Conference on Computer Vision and Pattern Recognition*, pages 1363–1370, Jun 2010.

[10] S. Haker, L. Zhu, A. Tannenbaum, and S. Angenent. Optimal mass transport for registration and warping. *International Journal of Computer Vision*, 60(3):225–240, 2004.

[11] B. Horn and B. Schunck. Determining optical flow. *Artificial intelligence*, 17, 1981.

[12] X. Liu, K. Abd-Elmoniem, and J. Prince. Incompressible cardiac motion estimation of the left ventricle using tagged mr images. *Medical Image Computing and Computer-Assisted Intervention*, 2009.

[13] D. Mumford and J. Shah. Optimal approximations by piecewise smooth functions and associated variational problems. *Communications on pure and applied mathematics*, 42(5):577–685, 1989.

[14] N. Paragios, M. Rousson, and V. Ramesh. Knowledge-based registration & segmentation of the left ventricle: a level set approach. In *Workshop Applications of Computer Vision*, 2002.

[15] S. Song and R. Leahy. Computation of 3-d velocity fields from 3-d cine ct images of a human heart. *IEEE Trans. Medical Imaging*, 10(3):295–306, 1991.

[16] G. Unal and G. Slabaugh. Coupled pdes for non-rigid registration and segmentation. In *Computer Vision and Pattern Recognition. Conference on*, 2005.

[17] A. Yezzi, L. Zollei, and T. Kapur. A variational framework for joint segmentation and registration. In *Mathematical Methods in Biomedical Image Analysis. IEEE Workshop on*, 2001.

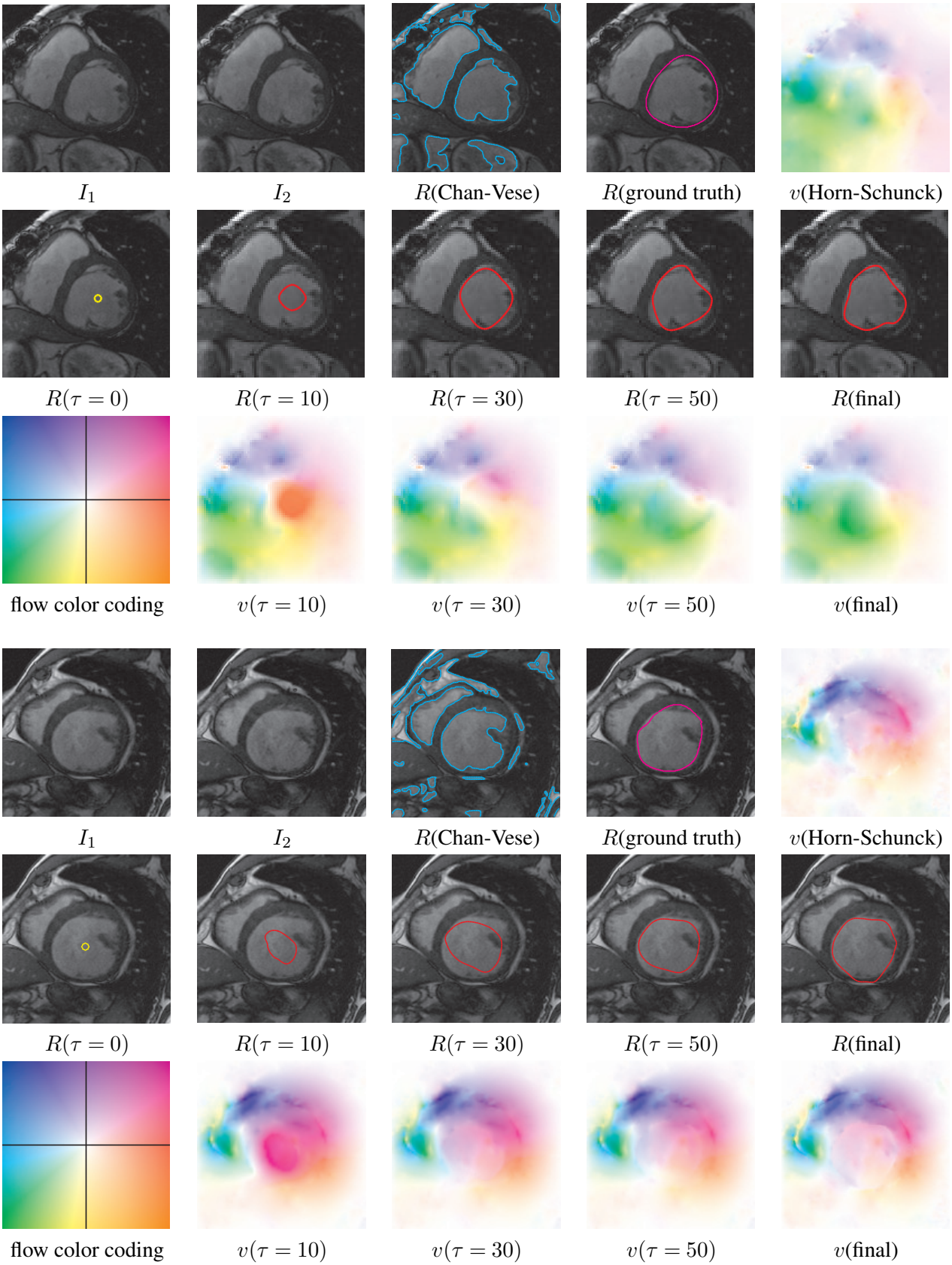


Figure 1: This figure shows the segmentation of the left ventricle from a sequence of cardiac MRI data. (Top tow) image $I_1$, image $I_2$, segmentation result by the Chan-Vese method, ground truth for the left ventricle region, optical flow by Horn-Schunck model. (Middle row) segmenting curve initialization, snapshots of the segmenting curve evolution in time and the final segmentation of the left ventricle by our method. (Bottom row) standard color coding scheme for the optical flow, snapshot of the deformation field evolution in time, and the final deformation field by our method. See text for assessment of the results.